ASM Sc. J., 13, Special Issue 2, 2020 for ICSCC2019, 56-67

Deep Analysis of Full Battery Energy Stored Quasi Z Source Inverter across All DC Capacitors' Terminal

Sia Yew Wei* and Law Kah Haw

[1]*Department of Electrical and Computer Engineering, Curtin University*

CDT 250, 98009 Miri, Sarawak, Malaysia

Quazi Z-Source Inverter (qZSI) is a cost efficient power converter/inverter built in single stage topology. It provides several advantages over the conventional power converters such as being able to perform buck and boost conversion without needing additional switching devices to reduce power loss. In addition, the existing qZSI can boost its output to be as twice amount of the input source voltage with the similar duty ratio. Knowing that inconsistent solar irradiation and temperature will cause fluctuating DC voltage produced by solar photovoltaic (PV) system, hence, this paper proposed full Battery Energy Storage System (BESS) across all DC capacitors' terminal of qZSI. The proposed control scheme with battery current controller, battery management and electronic circuit breaker (ECB) algorithm is also introduced in this paper to ensure continuous conduction mode (CCM) operation for the proposed qZSI. Furthermore, the effectiveness of battery charging and discharging of proposed qZSI with battery connected parallel at capacitor-1 C_1 and capacitor-2, C_2 are deeply analyzed and compared via the proposed control scheme. All mathematical derivation of proposed qZSI and control scheme is clearly presented in this paper. It is concluded that qZSI with battery connected across capacitor-1, C_1 is more preferable for high power industrial applications due to its wider power discharging range and able to buffer and smoothen the variable PV input voltage and power to load demand.

Keywords: Quasi Z-Source Inverter (qZSI); Maximum Power Point Tracking (MPPT)

I. INTRODUCTION

Nowadays, the application of qZSI has been widely exploited to the PV power system based on renewable solar energy sources (Rekha *et al.*, 2017; Law *et al.*, 2019a). Due to its unique characteristic, it has several advantages over the other conventional power converter with two-stage topologies, which is 1) able to perform buck-boost power conversion in a single stage topology 2) no additional switching devices is required 3) low construction and material cost 4) low voltage stress 5) lower I^2R power loss and higher efficiency 6) able to be controlled to achieve four quadrant operation (i.e., DC-DC, DC-AC, AC-DC and AC-DC power conversion) (Ayad 2017; Law *et al.*, 2011; 2012; 2014a; 2014b; 2019b; 2019c; 2019d; 2019e). However, there is unstable voltage/power generated from the PV system due to inconsistent of solar irradiance and temperature during the day (Ge *et al.*, 2013). Therefore, qZSI with battery energy storage system (BESS) is proposed to the PV system, which provides several advantages during DC-AC power boost conversion such as 1) buffer and smoothen the fluctuation of PV input voltage/power to grid/load 2) store excessive PV input power 3) supply energy to compensate the low PV power generated to high load demand (Liu *et al.*, 2014).

According to (Liu *et al.*, 2014), PV grid-tie BESS-qZSI topology is proposed to allow stable and smoothen grid power generation. The existing control scheme for battery energy management in terms of PI controllers and maximum power point tracking (MPPT) to regulate and store the power (Law *et al.*, 2019f). Moreover, it can utilize the battery

*Corresponding author's e-mail: siayewwei96@gmail.com

efficiently and prevent it from overcharge and discharge to save its lifetime. The proposed PI-based current dual loop controller is to manage the state of charge (SOC) of the battery. The small signal modeling of the BESS-qZSI topology was taken into consideration to counter the non-linear characteristic and provide convenience in the controller design. The switching element of the aforementioned topology was driven and modulated through space-vector-pulse-width-modulation (SVPWM) technique. (Liu *et al.*, 2013) demonstrated the further contributed work from (Liu *et al.*, 2012) to get unity power factor with P-Q coupling controller. The BESS-qZSI was further enhanced in the form of multi-level cascaded and control scheme-based phase-shift-SPWM (PS-SPWM) switching at effective switching frequency 10 kHz (Ge *et al.*, 2017; Khajesalehi *et al.*, 2015). However, the energy-management control scheme for qZSI with a battery connected at two different non-DC link capacitor, and unipolar carrier-based sinusoidal-pulse-width-modulation (SPWM) technique and its effective switching frequency were not revealed from the work. Furthermore, CCM and discontinuous conduction mode (DCM) analysis of BESS-qZSI with battery power charging and discharging capabilities in SOC management were not further discussed.

The main contributions of this paper are to develop a control scheme for the proposed dynamic model BESS-qZSI topology with a battery connected parallel either at two different capacitors. The control method with battery current controller, battery management and ECB are to ensure the battery charge or discharge while maintaining the system to work in CCM. Moreover, it can protect the battery life from over-charging and over-discharging. To achieve the desired AC output voltage waveform, a unipolar carrier based pulse width modulation (CB-PWM) is applied in this work. The arrangement of this paper is as follows: Section II demonstrate the small-signal model of BESS-qZSI and its control scheme; Section III and IV are presented the analyzed simulation results and conclusion for this project.

II. MATERIALS AND METHOD

A. Small-Signal Modelling of Battery Based QZSI

In Figures 1(a) and 1(b), it shows the proposed small signal model of energy-stored qZSI topology where only one battery connected in parallel with the capacitor C_1 and C_2, respectively.

Both the proposed energy stored qZSI topology has similar two operating modes discovered from the conventional qZSI; which are, shoot-through state and non-shoot-through state in CCM (Yong *et al.*, 2018; Ong *et al.*, 2017). In shoot-through mode, cross conduction occurs across S_1 and S_2 or S_3 and S_4 of the H-bridge inverter to reverse bias the diode and charge up the inductors. In non-shoot-through mode, conduction occurs through S_1 and S_4 or S_2 and S_3 allowing continuous current from the source voltage V_P and the inductors (i.e., L_1 and L_2) to flow through the diode, charge the capacitors, and drive the load.

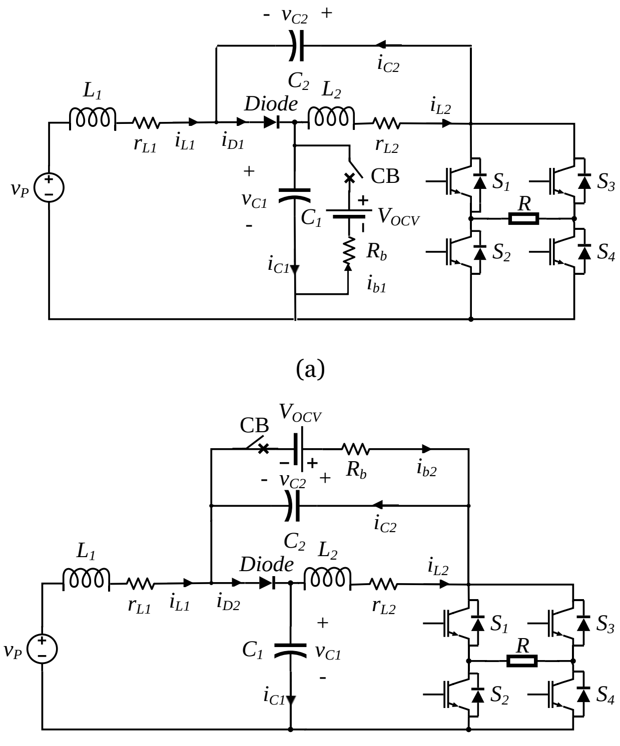

(a)

(b)

Figure 1. Small-signal model of the qZSI topology in non-shoot-through state with (a) battery V_{b1} connected at parallel at the capacitor C_1 and (b) battery V_{b2} connected parallel at the capacitor C_2.

To analyze the small-signal model of energy-stored qZSI, the battery voltage V_b (i.e., the summation of the open-circuit voltage V_{ocv} and the voltage drop across the battery's internal resistance R_b) which paralleled to capacitor C_1 or C_2 and the equivalent series resistance (ESR) of each inductors (i.e., r_{L1}

and r_{L2}) are considered. The ESR of each capacitor, however, is neglected to simplify the controller parameter design in the next section. The quality performance of the battery current closed-loop control still can be ensured without capacitor's ESR (Liu et. al 2014). For qZSI with battery across capacitor C_1 or C_2, the relationship between the aforementioned parameters are derived in (1) and (2) for Figures 1(a) and 1(b), respectively, as follow:

$$v_{C1} = V_{b1} = V_{OCV} - R_b i_{b1} \qquad \dot{v_{C1}} = -R_b \dot{i_{b1}} \tag{1}$$

$$v_{C2} = V_{b2} = V_{OCV} - R_b i_{b2} \qquad \dot{v_{C2}} = -R_b \dot{i_{b2}} \tag{2}$$

Assuming $r_{L1} = r_{L2}$, the state space equations (i.e., in matrix form) for the shoot-through state (i.e., *D*) and non-shoot-through state (i.e., *1-D*) together with the relationship of the aforementioned parameters are attained in (3) and (4) for qZSI with battery across capacitor C_1, as well as (5) and (6) for battery across capacitor C_2, respectively (Law 2018); where V_{PN} is the DC-link voltage, I_{PN} is DC-link current, I_{L1} and I_{L2} are the current flows through inductor L_1 and L_2, respectively, and V_{C1} and V_{C2} are the voltages measured across capacitor C_1 and C_2.

By substituting *D* and (1-*D*) into (3) and (5) as well as (4) and (6), respectively, the average dynamic state equations for qZSI with battery across capacitor C_1 or C_2 are derived in (7) and (8).

Under steady-state condition, the relevant steady-state parameters are found and derived in (9)-(15) by considering the left side of (7) and (8) is equal to zero as follows:

Battery at C_1:

$$V_{PN} = 2V_{b1} - V_P \qquad I_{L2} - I_{L1} = I_{b1} \tag{9}$$

$$I_{PN} = \frac{(1-2D)I_{L1} + (1-D)I_{b1}}{1-D} \tag{10}$$

Battery at C_2:

$$V_{PN} = 2V_{b2} + V_P \qquad I_{L1} - I_{L2} = I_{b2} \tag{11}$$

$$I_{PN} = \frac{(1-2D)I_{L1} + DI_{b2}}{1-D} \tag{12}$$

Battery at C_1 or C_2:

$$V_{C1} = V_{C2} + V_P \qquad V_{PN} = V_{C1} + V_{C2} \tag{13}$$

$$V_{C1} = \frac{1-D}{1-2D}V_P \qquad V_{C2} = \frac{D}{1-2D}V_P \tag{14}$$

$$\beta = \frac{V_{PN}}{V_P} = \frac{1}{1-2D} \tag{15}$$

where β is the boost factor of the qZSI in (15) and the shoot-through duty ratio *D* in the steady-state must not bigger or equal to 0.5 to allow the DC-link voltage V_{PN} remain in finite range.

By taking small deviation of state variables from operating point and then applied Laplace transform to (7) and (8), the dynamic small-signal model for both the energy-stored qZSI topology is derived in (16) and (17) (Ong *et al.*, 2017); where $I_{11} = I_{PN} - I_{b1} - 2I_{L1}$, $I_{22} = I_{PN} + I_{b2} - 2I_{L1}$, $V_{11} = V_{C2} + V_{OCV} - R_bI_{b1}$ and $V_{22} = V_{C1} + V_{OCV} - R_bI_{b2}$.

Battery at capacitor C_1:

$$\begin{bmatrix} L_1 & 0 & 0 & 0 \\ 0 & L_2 & 0 & 0 \\ 0 & 0 & R_bC_1 & 0 \\ 0 & 0 & 0 & C_2 \end{bmatrix}\begin{bmatrix} \dot{i_{L1}} \\ \dot{i_{L2}} \\ \dot{i_{b1}} \\ \dot{v_{C2}} \end{bmatrix} = \begin{bmatrix} -r_L & 0 & 0 & 1 \\ 0 & -r_L & -R_b & 0 \\ 0 & 1 & -1 & 0 \\ -1 & 0 & 0 & 0 \end{bmatrix}\begin{bmatrix} i_{L1} \\ i_{L2} \\ i_{b1} \\ v_{C2} \end{bmatrix} + \begin{bmatrix} 1 & 0 & 0 \\ 0 & 0 & 1 \\ 0 & 0 & 0 \\ 0 & 0 & 0 \end{bmatrix}\begin{bmatrix} v_P \\ i_{PN} \\ v_{OCV} \end{bmatrix} \tag{3}$$

$$\begin{bmatrix} L_1 & 0 & 0 & 0 \\ 0 & L_2 & 0 & 0 \\ 0 & 0 & R_bC_1 & 0 \\ 0 & 0 & 0 & C_2 \end{bmatrix}\begin{bmatrix} \dot{i_{L1}} \\ \dot{i_{L2}} \\ \dot{i_{b1}} \\ \dot{v_{C2}} \end{bmatrix} = \begin{bmatrix} -r_L & 0 & R_b & 0 \\ 0 & -r_L & 0 & -1 \\ -1 & 0 & -1 & 0 \\ 0 & 1 & 0 & 0 \end{bmatrix}\begin{bmatrix} i_{L1} \\ i_{L2} \\ i_{b1} \\ v_{C2} \end{bmatrix} + \begin{bmatrix} 1 & 0 & -1 \\ 0 & 0 & 0 \\ 0 & 1 & 0 \\ 0 & -1 & 0 \end{bmatrix}\begin{bmatrix} v_P \\ i_{PN} \\ v_{OCV} \end{bmatrix} \tag{4}$$

Battery at capacitor C_2:

$$\begin{bmatrix} L_1 & 0 & 0 & 0 \\ 0 & L_2 & 0 & 0 \\ 0 & 0 & C_1 & 0 \\ 0 & 0 & 0 & R_bC_2 \end{bmatrix}\begin{bmatrix} \dot{i_{L1}} \\ \dot{i_{L2}} \\ \dot{v_{C1}} \\ \dot{i_{b2}} \end{bmatrix} = \begin{bmatrix} -r_L & 0 & 0 & -R_b \\ 0 & -r_L & 1 & 0 \\ 0 & -1 & 0 & 0 \\ 1 & 0 & 0 & -1 \end{bmatrix}\begin{bmatrix} i_{L1} \\ i_{L2} \\ v_{C1} \\ i_{b2} \end{bmatrix} + \begin{bmatrix} 1 & 0 & 1 \\ 0 & 0 & 0 \\ 0 & 0 & 0 \\ 0 & 0 & 0 \end{bmatrix}\begin{bmatrix} v_P \\ i_{PN} \\ v_{OCV} \end{bmatrix} \tag{5}$$

$$\begin{bmatrix} L_1 & 0 & 0 & 0 \\ 0 & L_2 & 0 & 0 \\ 0 & 0 & C_1 & 0 \\ 0 & 0 & 0 & R_bC_2 \end{bmatrix}\begin{bmatrix} \dot{i_{L1}} \\ \dot{i_{L2}} \\ \dot{v_{C1}} \\ \dot{i_{b2}} \end{bmatrix} = \begin{bmatrix} -r_L & 0 & -1 & 0 \\ 0 & -r_L & 0 & R_b \\ 1 & 0 & 0 & 0 \\ 0 & -1 & 0 & 0 \end{bmatrix}\begin{bmatrix} i_{L1} \\ i_{L2} \\ v_{C1} \\ i_{b2} \end{bmatrix} + \begin{bmatrix} 1 & 0 & 0 \\ 0 & 0 & -1 \\ 0 & -1 & 0 \\ 0 & 1 & 0 \end{bmatrix}\begin{bmatrix} v_P \\ i_{PN} \\ v_{OCV} \end{bmatrix} \tag{6}$$

Battery at capacitor C_1:

$$\begin{bmatrix} L_1 & 0 & 0 & 0 \\ 0 & L_2 & 0 & 0 \\ 0 & 0 & R_bC_1 & 0 \\ 0 & 0 & 0 & C_2 \end{bmatrix}\begin{bmatrix} \dot{i_{L1}} \\ \dot{i_{L2}} \\ \dot{i_{b1}} \\ \dot{v_{C2}} \end{bmatrix} = \begin{bmatrix} -r_L & 0 & (1-D)R_b & D \\ 0 & -r_L & -DR_b & D-1 \\ D-1 & D & -1 & 0 \\ -D & 1-D & 0 & 0 \end{bmatrix}\begin{bmatrix} i_{L1} \\ i_{L2} \\ i_{b1} \\ v_{C2} \end{bmatrix} + \begin{bmatrix} 1 & 0 & D-1 \\ 0 & 0 & D \\ 0 & 1-D & 0 \\ 0 & D-1 & 0 \end{bmatrix}\begin{bmatrix} v_P \\ i_{PN} \\ v_{OCV} \end{bmatrix} \tag{7}$$

Battery at capacitor C_2:

$$\begin{bmatrix} L_1 & 0 & 0 & 0 \\ 0 & L_2 & 0 & 0 \\ 0 & 0 & C_1 & 0 \\ 0 & 0 & 0 & R_bC_2 \end{bmatrix}\begin{bmatrix} \dot{i_{L1}} \\ \dot{i_{L2}} \\ \dot{v_{C1}} \\ \dot{i_{b2}} \end{bmatrix} = \begin{bmatrix} -r_L & 0 & D-1 & -DR_b \\ 0 & -r_L & D & (1-D)R_b \\ 1-D & -D & 0 & 0 \\ D & D-1 & 0 & -1 \end{bmatrix}\begin{bmatrix} i_{L1} \\ i_{L2} \\ v_{C1} \\ i_{b2} \end{bmatrix} + \begin{bmatrix} 1 & 0 & D \\ 0 & 0 & D-1 \\ 0 & D-1 & 0 \\ 0 & 1-D & 0 \end{bmatrix}\begin{bmatrix} v_P \\ i_{PN} \\ v_{OCV} \end{bmatrix} \tag{8}$$

Battery at capacitor C_1

$$\begin{cases} (Ls + r_L)\widetilde{\imath_{L2}}(s) = (D-1)\widetilde{v_{C2}}(s) - DR_b\widetilde{\imath_{b1}}(s) + D\widetilde{v_{OCV}}(s) + V_{11}\tilde{d}(s) \\ (R_bCs + D)\widetilde{\imath_{b1}}(s) = (2D-1)\widetilde{\imath_{L2}}(s) + (1-D)\widetilde{\imath_{PN}}(s) - I_{11}\tilde{d}(s) \\ Cs\widetilde{v_{C2}}(s) = (1-2D)\widetilde{\imath_{L2}}(s) + D\widetilde{\imath_{b1}}(s) + (D-1)\widetilde{\imath_{PN}}(s) + I_{11}\tilde{d}(s) \end{cases} \quad (16)$$

Battery at capacitor C_2

$$\begin{cases} (Ls + r_L)\widetilde{\imath_{L1}}(s) = (D-1)\widetilde{v_{C1}}(s) - DR_b\tilde{\imath}_b(s) + \widetilde{v_P}(s) + D\widetilde{v_{OCV}}(s) + V_{22}\tilde{d}(s) \\ Cs\widetilde{v_{C1}}(s) = (1-2D)\widetilde{\imath_{L1}}(s) + D\widetilde{\imath_{b2}}(s) + (D-1)\widetilde{\imath_{PN}}(s) + I_{22}\tilde{d}(s) \\ (R_bCs + D)\widetilde{\imath_{b2}}(s) = (2D-1)\widetilde{\imath_{L1}}(s) + (1-D)\widetilde{\imath_{PN}}(s) - I_{22}\tilde{d}(s) \end{cases} \quad (17)$$

Each upper-case variable (e.g., I_{L1}) and lower-case variable with tilde (e.g., $\widetilde{\imath_{L1}}$) defines as the the steady-state operating point and the small-signal disturbance, respectively.

By equating (16) and (17) and then neglect the other small signal perturbance (e.g., $\widetilde{v_P}, \widetilde{v_{ocv}}$ *and* $\widetilde{\imath_{PN}}$), the small-signal based transfer function for qZSI with battery across capacitor C_1 or C_2 that relates to the battery current $\tilde{\imath}_b$ and the shoot-through duty ratio $\tilde{d}$ is derived, respectively, as follow:

Battery at C_1

$$G_{\widetilde{I_{b1}}\tilde{d}} = \frac{\widetilde{\imath_{b1}}(s)}{\tilde{d}(s)} = \frac{-sLI_{11} - r_LI_{11} + (2D-1)V_{11}}{s^2CLR_b + s(CR_br_L + DL) + Dr_L + R_b(1-2D)^2} \quad (18)$$

Battery at C_2

$$G_{\widetilde{I_{b2}}\tilde{d}} = \frac{\widetilde{\imath_{b2}}(s)}{\tilde{d}(s)} = \frac{-sLI_{22} - r_LI_{22} + (2D-1)V_{22}}{s^2CLR_b + s(CR_br_L + DL) + Dr_L + R_b(1-2D)^2} \quad (19)$$

From (18) and (19), it is clarified that the qZSI topology with battery connected parallel at capa citor C_1 or C_2 have a similar type of transfer function. The main purpose of derived transfer function is to build the controller for the battery current closed-loop control.

B. Control Scheme

In Figure 2, it shows the control scheme for the energy-stored qZSI topology with battery connected parallel at capacitor C_1 or C_2.

The control scheme includes a battery ECB algorithm, battery current controller, and battery management algorithm. In this scenario, it is noted that there is only proportional (P) controller designed for the built circuit model. It is to differentiate and analyze the unique characteristic of two different types of energy-stored qZSI circuit model with the battery across either capacitor C1 or C2 for its battery charging and discharging capabilities in the simulation.

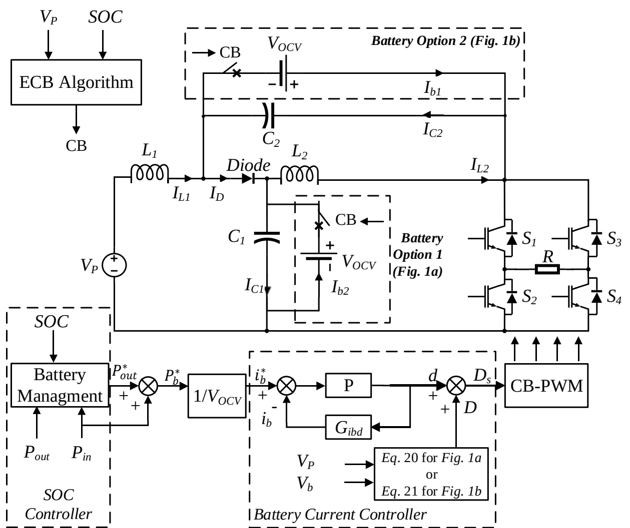

Figure 2. The control scheme for the energy-stored qZSI topology with battery connected parallel at capacitor C_1 or capacitor C_2.

From Figure 2, the small-signal shoot-through duty ratio *d* is tracked from the closed-loop of battery current controller via the P controller. It is then added with the steady-state shoot-through duty ratio *D* from the feed-forward controller to get the desired shoot-through duty ratio D_s. The final duty ratio D_s is forward to the modulator with unipolar CB-PWM technique for simple boost control.

The steady-state shoot-through duty ratio for qZSI topology with battery connected parallel at capacitor C_1 or C_2 are derived in (20) and (21), respectively, as follow:

Battery at capacitor C_1

$$D = \frac{V_b - V_P}{2V_b - V_P} \quad (20)$$

Battery at capacitor C_2

$$D = \frac{V_b}{2V_b + V_P} \quad (21)$$

1. Battery Managemenet

In Figure 3, it depicts the battery management algorithm framework for the energy-stored qZSI topology. Equations (22), (23), and (24) derive the DC input power P_{in}, battery power P_b, and the AC output power P_{out}, respectively. If other powers are controlled, then one of the power value can be determined. However, V_{PN} is uncontrollable which is oscillates with V_P.

$$P_{in} = V_P \times I_{L1} \tag{22}$$

$$P_b = V_b \times I_b \tag{23}$$

$$P_{out} = P_{in} + P_b = V_{out} \times I_{out} = D \times 0 + (1-D)V_{PN}I_{out} \tag{24}$$

$$V_{out} = (1-D)V_{PN} = \frac{1-D}{1-2D}V_P \tag{25}$$

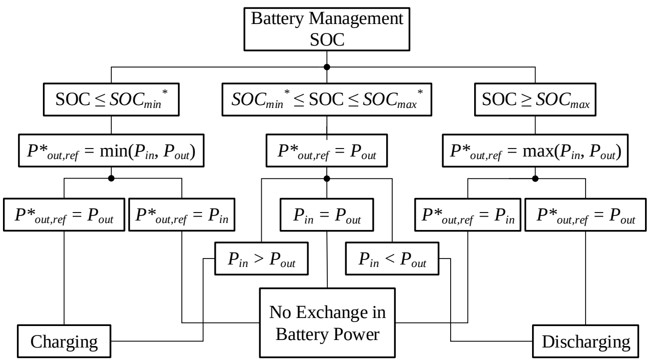

Figure 3. Battery State of Charge SOC control algorithm.

$$V_{out} = (1-D)V_{PN} = \frac{1-D}{1-2D}V_P \tag{25}$$

$$I_{out} = \frac{V_{out}}{R} = \frac{(1-D)V_{PN}}{R} \tag{26}$$

where R is defined as a load resistance, V_{out} and I_{out} in (25) and (26), respectively, are the output voltage and current for the output power.

From the battery state of charge (SOC) controller shown in Figure 3, the battery power cannot be over-discharged lower than the lower limit of SOC (i.e., SOC_{min}^*) and overcharged higher than the upper limit of SOC (i.e., SOC_{max}^*). Therefore, the input power, output power as well as the output power reference $P_{out,ref}^*$ and battery power reference $P_{b,ref}^*$ derived in (27) and (28), respectively, are taken into the consideration for the comparison and controlling purpose.

$$P_{out,ref}^* = P_{out} - P_{in} \tag{27}$$

$$P_{b,ref}^* = P_{out,ref}^* - P_{in} \tag{28}$$

There are three main operating cases for the SOC of battery, which are:

Case 1: When the SOC of the battery is exceeded its upper limit SOC_{max}^*, the battery power is discharging if $P_{b,ref}^* > 0$ (i.e., $P_{out,ref}^* = P_{out}$) while there is no power exchange for the battery if $P_{b,ref}^* = 0$ (i.e., $P_{out,ref}^* = P_{in}$).

Case 2: When the SOC of the battery is less than its lower limit SOC_{min}^*, the battery power is charging if $P_{b,ref}^* < 0$ (i.e., $P_{out,ref}^* = P_{out}$) while there is no power exchange for the battery if $P_{b,ref}^* = 0$ (i.e., $P_{out,ref}^* = P_{in}$).

Case 3: When the SOC of the battery reaches between the range of its lower limit SOC_{min}^* and upper limit SOC_{max}^*, the battery is performed similar power exchanging characteristic tabulated in Table 1.

Table 1. Comparison of Inductors Current Behavior

Mode	Input and Output Power Relationship	Battery Power	Inductor Currents	
			Battery at C_1	Battery at C_2
1	$P_{in} < P_{out}$	$P_b > 0$ (discharging)	$I_{L1} < I_{L2}$	$I_{L1} > I_{L2}$
2	$P_{in} = P_{out}$	$P_b = 0$ (no power exchange)	$I_{L1} = I_{L2}$	$I_{L1} = I_{L2}$
3	$P_{in} > P_{out}$	$P_b < 0$ (charging)	$I_{L1} > I_{L2}$	$I_{L1} < I_{L2}$

Based on the equations for inductor currents and battery current from (9), (11), and (22)-(24), the battery power and inductor current behaviors for qZSI with battery connected parallel at capacitor C_1 and C_2 are classified into three cases for $P_{in} > P_{out}$, $P_{in} = P_{out}$, and $P_{in} < P_{out}$ as shown in Table 1 which also can be realized from Figure 3.

2. Battery Electronic Circuit Breaker Algorithm

As clarified earlier, DC input voltage source was used to represent the PV panel and hence MPPT in the system is ignored. As there is only P controller introduced in this scenario to identify the characteristics between two different types of energy-stored qZSI, the system is difficult to limit the battery from over-charging and over-discharging due to the constant duty ratio produced from the feed-forward equation. Therefore, the new ECB algorithm for qZSI circuit model is introduced to protect the battery life from over-charging and over-discharging. An ECB is connected in series with the battery across capacitor C_1 and capacitor C_2 as depicted in Figures 1(a) and 1(b). Its algorithm is elaborated in Figure 4.

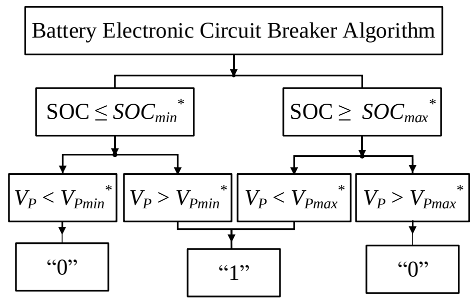

Figure 4. Battery Electronic Circuit Breaker ECB algorithm

There are two operating states resulted from ECB algorithm, which are normally open (NO) state and normally closed (NC) state indicating by “0” and “1”, respectively. These operating modes are functioning according to both the SOC of the battery and the DC input voltage with its references (i.e., SOC_{min}^*, SOC_{max}^*, V_{Pmin}^* and V_{Pmax}^*).

3. *Battery Charging and Discharging Capabilities in CCM*

The inequality of the battery voltage, current, and power for its charging and discharging capabilities to work in CCM during boost control are derived as shown in Table 2 and 3.

Table 2. Comparison of Battery Voltage Boost Control Range Behaviour

Cases	Battery voltage range for boost control to work in CCM		
	Input and battery voltage relationship	Duty ratio	Boost factor
Battery at C_1	$V_P < V_b < \infty$	$0 < D < 0.5$	$1 < \beta < \infty$
Battery at C_2	$0 < V_b < \infty$		

By equating (20) and (21) into Table 2, it classified the battery voltage range required for qZSI with battery connected parallel at capacitor C_1 and C_2 to work in CCM during boost control. It is noted that qZSI with battery at capacitor C_2 can be used to high input voltage than the battery voltage (i.e., $V_P > V_b$) and can always work in the CCM during battery charging compared to battery at capacitor C_1.

In addition, qZSI with battery across capacitor C_1 or C_2 work in CCM during non-shoot-through mode when the diode current is forward biased are derived in (29) and (30), respectively, as below:

$$i_{D1} = i_{L2} - i_{b1} + i_{C1} > 0 \quad (29)$$

$$i_{D2} = i_{L1} - i_{b2} + i_{C2} > 0 \quad (30)$$

Otherwise, it works in DCM if $i_D \le 0$ during the non-shoot-through mode.

In steady state, the average capacitor current I_{C1} and I_{C2} is equal to zero for (29) and (30). Therefore, the inequality for the battery discharging power and current to work in CCM is derived as shown in Table 3. It is noted that qZSI with battery at capacitor C_2 has limited battery power discharging to ensure the system work in CCM (i.e., $P_b < \frac{D}{1-2D} P_{in}$ or $P_b < \frac{D}{1-D} P_{out}$). Hence, qZSI with battery at capacitor C_1 has a wider battery power discharging range compare to battery at capacitor C_2. Therefore, it can always work in the CCM during battery discharging as long as there is input power (ie., $0 < P_{in}$) during power conversion and the amount of battery discharging power is smaller than the load demand (ie., $P_b < P_{out}$).

Table 3. Comparison of Battery Discharging Power And Current Range Behaviour In Steady State

Cases	Battery discharging power and current range to work in CCM in steady state		
	Inequality of battery power to input power or output power relationship	Battery current and inductor current relationship	Diode current
Battery at C_1	$0 < P_{in}$ or $P_b < P_{out}$	$I_{b1} < I_{L2}$ or $I_{L1} > 0$	$I_D > 0$
Battery at C_2	$P_b < \frac{D}{1-2D} P_{in}$ or $P_b < \frac{D}{1-D} P_{out}$	$I_{b2} < I_{L1}$ or $I_{L2} > 0$	

As from Figure 3, the battery power depends on the input power and battery SOC. To counter the DCM happens in the system when qZSI with battery at capacitor C_1 being over-charging and battery at capacitor C_2 being over-discharging, the proposed battery management and ECB algorithm allow the system to work in CCM with fulfilled criteria in Table 2 and 3.

After the comparison between qZSI with battery connected parallel at capacitor C_1 and capacitor C_2, it is notified that battery across capacitor C_1 is more preferable for power conversion in high power generation system. Due to its larger capacity of BESS can be applied and always controlled in the CCM during battery charging and discharging in the system as long as the total series-connected battery voltage is larger than the input voltage (ie., $V_P < V_b$).

III. RESULT AND DISCUSSION

A. Simulation results

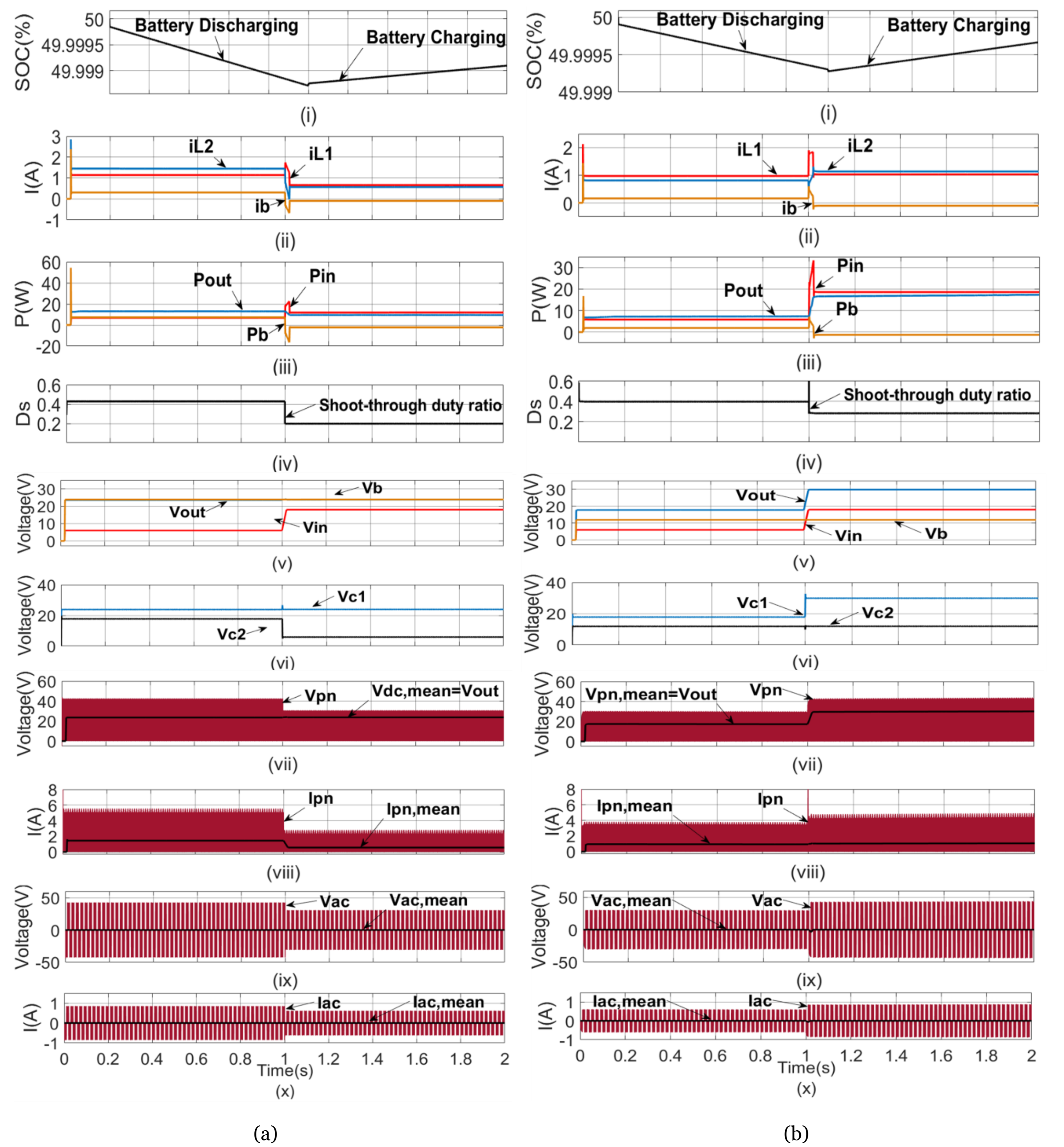

Figure 5. Simulation results when $SOC_{min}^* \leq$ SOC $\leq SOC_{max}^*$ with (a) battery V_{b1} connected at parallel at the capacitor C_1 and (b) battery V_{b2} connected parallel at the capacitor C_2, i) battery SOC, ii) battery and inductor currents, iii) DC input power, DC output power, and battery power, iv) shoot-through duty ratio D, v) DC input voltage, DC output voltage, and battery voltage, vi) capacitors voltage, vii) DC-link voltage, viii) DC-link current, ix) AC output voltage, x) AC output current

The proposed two different energy-stored qZSI topologies shown in Figure 2 were tested through MATLAB/SIMULINK simulation that run in 2 s. It is to validate the theoretical findings of battery charging and discharging capabilities.

In the simulation, there were three scenarious to be analyse: 1) battery charging and discharging regimes, 2) battery over-charging prevention and 3) battery over-discharging prevention. All the system specifications were shown in Table 4. The P parameter for the control of the battery current closed-loop was autotuned via MATLAB/SIMULINK simulation with the transfer function derived in the previous section.

Table 4. System Parameters

Circuit parameters	**Value**
DC voltage source, V_P	6 V, 12 V, 18 V
Battery voltage V_{b1} and V_{b2}	24V and 12 V
Battery internal resistor R_b	1.37 Ω
Energy-stored qZSI inductance of L_1 and L_2	0.1 mH
Parasitic resistance of inductor r_1 and r_2	0.15 Ω
Energy-stored qZSI capacitance of C_1 and C_2	1.0 mF
Output load resistor R	50 Ω
Fundamental frequency	50 Hz
Switching frequency, f_{sw}	40 kHz
SOC_{min}^* and SOC_{max}^*	40 % and 80%

1. Battery Charging and Discharging Regimes

Throughout the simulation for the case of SOC_{min}^*<SOC< SOC_{max}^*, the battery SOC was set to 50 % while DC voltage source V_P was set with a step change from 6V to 18V at 1 s. Therefore, the battery is discharging at 0 s to 1 s (i.e., V_P =6V) then charging at 1 s to 2 s (i.e., V_P =18V) under same load condition as referred to battery SOC in Figure 5(i).

As from Figures 5(ii) and 5(iii), it show that the battery supply energy to compensate the low PV power generated to high load demand during battery discharging mode at 0 s to 1 s and store excessive input power during battery charging mode at 1 s to 2 s. Moreover, the relationship between the currents (i.e., I_{L1}, I_{L2}, and I_b) and powers (i.e., P_{in}, P_{out}, and P_b) behavior for two different types of proposed energy-stored qZSI shown in Figures 5(ii) and 5(iii) were proven and can be verified in Table 1. It is noted that the battery discharge with positive current when SOC decreases and charge with negative current when SOC increases.

On the other hand, energy-stored qZSI with battery across capacitor C_1 was found that the novel output power and voltage generated shown in Figures 5(a)(iii) and 5(a)(v) is very stable and remaining constant during both battery charging and discharging modes as compared to battery connected at capacitor C_2 in Figures 5(b)(iii) and 5(b)(v) with the proposed method. Furthermore, Figure 5(a)(iii) shows that its battery across capacitor C_1 has wider power discharging range and can always work in the CCM during battery discharging; which has proven and can be verified in Table 3. Therefore, qZSI with battery across capacitor C_1 is more preferable for industrial application in high power conversion system with its novel unique characteristic.

During the process, Figure 5(iv) shows the battery charging and discharging capabilities managed by the adjusted shoot-through duty ratio. The input/output/battery voltage, capacitors voltage, DC-link voltage and current, AC output voltage and current were shown in Figures 5(v) to 5(x), respectively. Note that the DC output voltage is taken from the mean value of DC-link voltage and it is also based on equation (25) and AC output voltage and current were presented in the form of 50Hz.

2. Battery Over-charging Prevention

Throughout the simualtion, given the upper limit of SOC is 80 % for the case of SOC≥ SOC_{max}^*. This is to investigate the battery over-charging prevention capability with the proposed control scheme in this scenario. Similar to the previous scenario, battery was set to discharge at 0 s to 1 s (i.e., V_P =6V) then it was charge at 1 s to 2 s (i.e., V_P =18V) under same load condition. The initial battery SOC was set to approximate 80 % as the battery was discharging in the beginning.

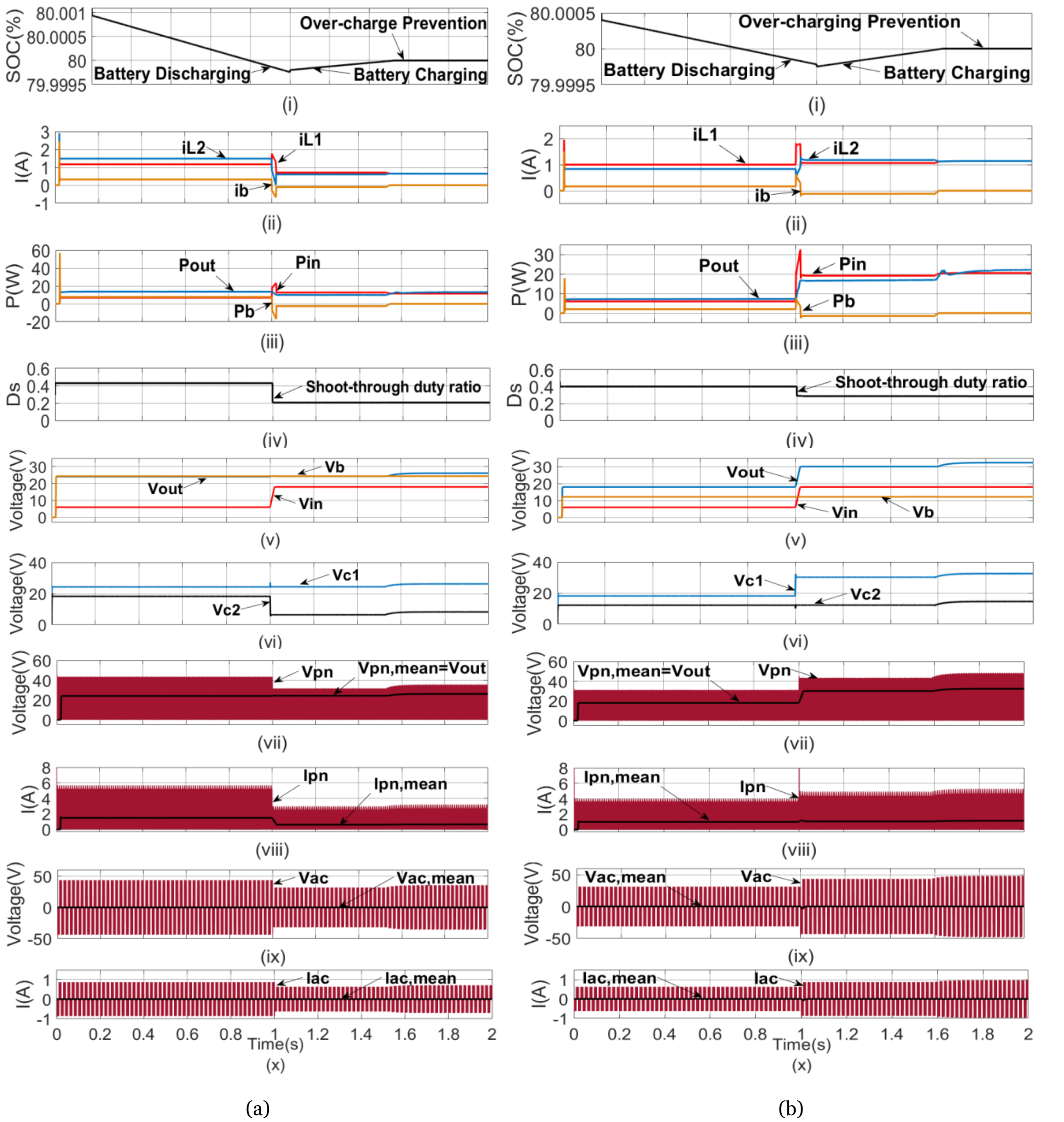

Figure 6. Simulation results when SOC≥ SOC_{max}^* with (a) battery V_{b1} connected at parallel at the capacitor C_1 and (b) battery V_{b2} connected parallel at the capacitor C_2, i) battery SOC, ii) battery and inductor currents, iii) DC input power, DC output power, and battery power, iv) shoot-through duty ratio D, v) DC input voltage, DC output voltage, and battery voltage, vi) capacitors voltage, vii) DC-link voltage, viii) DC-link current, ix) AC output voltage, x) AC output current

As from Figure 6(i), the control scheme avoid the battery being over-charging when the battery SOC reached 80 % and hence remaining constant at 1.6 s. Figures 6(ii) and (iii) show the inductor/battery current and input/output/battery power behaviour. The battery current and power become zero when the battery SOC is larger than 80 % after 1.6 s. Figure 6(iv) shows the adjusted shoot-through duty ratio. Figures 6 (v) to 6(x) show the input/output/battery voltage, capacitors voltage, DC-link voltage and current, AC output voltage and current.

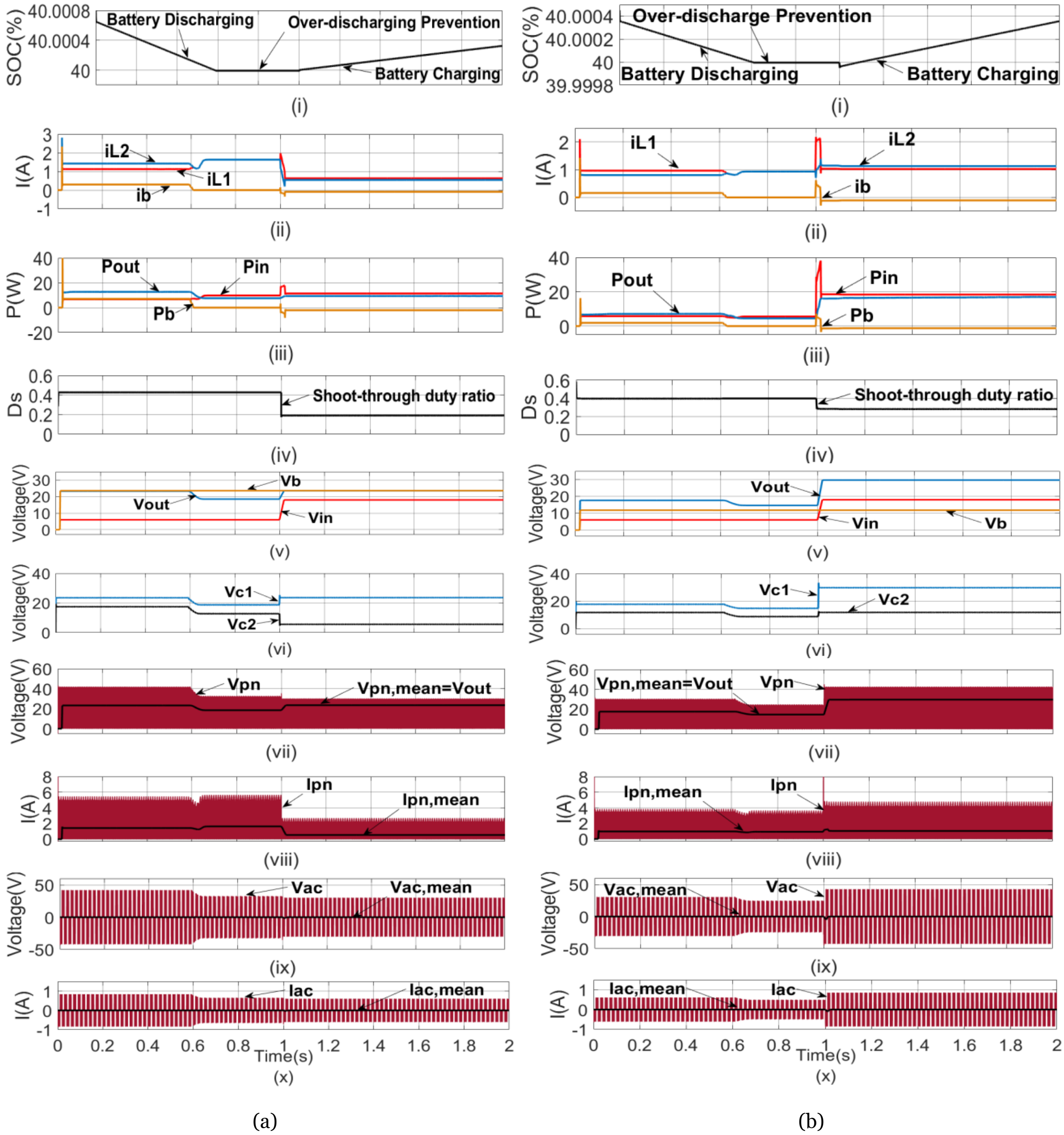

Figure 7. Simulation results when SOC≤ SOC_{min}^{*} with (a) battery V_{b1} connected at parallel at the capacitor C_1 and (b) battery V_{b2} connected parallel at the capacitor C_2, i) battery SOC, ii) battery and inductor currents, iii) DC input power, DC output power, and battery power, iv) shoot-through duty ratio D, v) DC input voltage, DC output voltage, and battery voltage, vi) capacitors voltage, vii) DC-link voltage, viii) DC-link current, ix) AC output voltage, x) AC output current

3. Battery Over-discharging Prevention

In this scenario, the lower limit of SOC was given to be 40 % for the case of SOC≤ SOC_{min}^{*} to test protection function of the control scheme when the battery SOC over-discharging to *40 %*. Similarly, DC voltage source V_P was set for the battery to discharge at 0 s to 1 s (i.e., V_P =6V) and charge at 1 s to 2 s (i.e., V_P =18V). The initial battery SOC was adjusted above 40 %.

In Figure 7(i), it shows that the prosed control scheme has stopped battery to discharge when the battery SOC closed to 40 % from 0.6 s to 1s. Figures 7(ii) and (iii) show the inductor/battery current and input/output/battery power behaviour. The battery current and power become zero when the battery SOC is smaller than 40 % from 0.6 s to 1s.

Figure 7(iv) shows the adjusted shoot-through duty ratio to manage battery. Figures 7(v) and 7(vi) show DC input voltage, DC output voltage, battery voltage and capacitors voltage. Figures 7(vii) to 7(x) show the DC-link voltage, DC-link current, AC output voltage and AC output current.

IV. CONCLUSION

This paper presented a control scheme for two different energy-stored qZSI topology. The proposed control scheme is structured with battery current controller, battery management algorithm, and the ECB algorithm. It is concluded that the battery successfully managed to charge and discharge effectively through the simulation analysis, as well as prevent the battery being over-charging and over-discharging. When comparing for two different type of the proposed energy-stored qZSI topology, the proposed method with the unique characteristic of the energy-stored qZSI when battery connected to capacitor C_1 is more reliable for industrial application in high power conversion system; where it shows novel in boosting constant output voltage and stabilize the output power with its wider battery discharging range, without the needs of MPPT algorithm to track the input voltage to constant reference value. Finally, the hypothesis of the experiment is accepted, where all the aforementioned advantages were realized via the simulation.

V. REFERENCES

Ayad, A. & Kennel, R. 2017, 'A comparison of quasi-z-source inverters and conventional two-stage inverters for pv applications', *EPE J.*, vol. 27, no. 2, pp. 43-59.

Ge, B., Haitham A.B., Peng, F.Z., Lei, Q., Almeida, A.T., Ferreira, F.J.T.E., Sun, D. & Liu, Y. 2013, 'An energy-stored quasi-z-source inverter for application to photovoltaic power system', *IEEE Trans. Ind. Electron.*, vol. 60, no. 10, pp. 4468-4481.

Ge, B., Liu, Y., Haitham A.B. & Peng, F.Z. 2017, 'State-of-charge balancing control for a battery-energy-stored quasi-z-source cascaded-multilevel-inverter based photovoltaic power system', *IEEE Trans. Ind. Electron.*, vol. 65, no. 3, pp. 2268–2279.

Khajesalehi, J., Sheshyekani, K., Hamzeh, M. & Afjei, E. 2015, 'High-performance hybrid photovoltaic -battery system based on quasi-z-source inverter: Application in microgrid', *IET Generation, Transmission Distribution*, vol. 9, no. 10, pp. 895–902.

Law, K.H. & Dahidah, M.S.A. 2014, 'DC-DC boost converter based MSHE-PWM cascaded multilevel inverter control for STATCOM systems', in *2014 International Power Electronics Conference*, 18 May 2014, Hiroshima, Japan.

Law, K.H. & Dahidah, M.S.A. 2014, 'New current control algorithm incorporating multilevel SHE-PWM approach for STATCOM operation under unbalanced condition', in *2014 IEEE 5th International Symposium on Power Electronics for Distributed Generation Systems*, 24 June 2014, Galway, Ireland.

Law, K.H. & Ng, W.P.Q. 2019, 'Dual closed-Loop scheme with lead compensator and proportional controller for quasi z-source inverter based STATCOM', in *2018 IEEE 7th International Conference Power and Energy*, 3 December 2018, Kuala Lumpur, Malaysia.

Law, K.H. 2019, 'Mathematics modelling and simulation of batteries charging capability in quasi Z source impedance network', in *7th International Conference on Smart Computing & Communications*, 28 June 2019, Sarawak, Malaysia.

Law, K.H., Dahidah, M. & Mariun, N. 2011, 'Cascaded multilevel inverter based statcom with power factor correction feature,' in *2011 IEEE Conference on Sustainable Utilization and Development in Engineering and Technology*, 20 October 2011, Semenyih, Malaysia.

Law, K.H., Dahidah, M., Sim, S.Y., Ng, W.P.Q., Masaoud, A. & Siada, A.A. 2019, 'An effective dual closed-loop scheme based on lead compensator and proportional controller for quasi z-source inverter', in *2018 IEEE Region 10 Conference*, 28 October 2018, Jeju, Korea.

Law, K.H., Dahidah, M.S.A., Konstantinou, G.S. & Agelidis, V.G. 2012, 'SHE-PWM cascaded multilevel converter with adjustable DC sources control for STATCOM applications', in *proceedings of the 7th International Power Electronics* *and Motion Control Conference*, 2 June 2012, Harbin, China.

Law, K.H., Loh, W.N. & Wong, K.I. 2019, 'Mathematics derivation and simulation modelling of maximum power point tracking based controller for quasi z source inverter', in *7th International Conference on Smart Computing & Communications*, 28 June 2019, Sarawak, Malaysia.

Law, K.H., Ng, W.P.Q. & Au, P.I. 2019, 'Design, Modelling and Control Implementation of PV-MPPT Based DC-DC Converter for STATCOM', *IOP Conference Series: Materials Science and Engineering*, vol. 495, iss. 1, pp. 012035.

Law, K.H., Ng, W.P.Q. & Au, P.I. 2019, 'Design, Modelling and Control Implementation of PV-MPPT Based DC-DC Converter for STATCOM', *IOP Conference Series: Materials Science and Engineering*, vol. 495, iss. 1, pp. 012035.

Liu, Y., Ge, B., Haitham Abu-Rub & Peng, F.Z. 2013, "Control system design of battery-assisted quasi-z-source inverter for grid-tie photovoltaic power generation," *IEEE Trans. Sustainable Energy*, vol. 4, no. 4, pp. 994– 1001.

Liu, Y., Ge, B., Haitham Abu-Rub, Atif Iqbal & Peng, F.Z. 2012, "Modeling and controller design of quasi-z-source inverter with battery based photovoltaic power system," *2012 IEEE Energy Convers. Congress and Exposition (ECCE)*, 15-20 September, 2012, pp. 3119–3124.

Liu, Y., Haitham Abu-Rub & Ge, B. 2014, "Z-source/quasi-z-source inverters: Derived networks, modulations, controls, and emerging applications to photovoltaic conversion," *IEEE Ind. Elect. Mag.*, vol. 8, no. 4, pp. 32-44.

Ong, J.S.X., Yong, K.S.K., Law, K.H., Ng, W.P.Q. & Dahidah, M. 2018, 'CCM and DCM analysis of quasi-z-source inverter', in *2017 IEEE Conference on Energy Conversion*, 30 October 2017, Kuala Lumpur, Malaysia.

Rekha, Y., Christopher, I., W. & Jamuna, V. 2017, "Quasi-zsi topology for renewable energy system: a review," *2017 Int. Conf. Power and Embedded Drive Cont.*, Chennai, India, 16-18 March, 2017, pp. 333-337.

Sia, Y.W. & Law, K.H. 2019, 'Deep analysis of quasi z source inverter for batteries charging and discharging capabilities across all DC capacitors' terminals', in *7th International Conference on Smart Computing & Communications*, 28 June 2019, Sarawak, Malaysia.

Yong, S.K., Law, K.H., Ng W.P.Q. & Dahidah, M. 2018, 'Lead compensator design for single-phase quasi Z-source inverter', *Journal of Telecommunication, Electronic and Computer Engineering*, vol. 10, iss. 1-12, pp. 39-44.